

Photometric study of strongly lensed high-redshift galaxies using JWST and HST

Arpita Ganguly¹

Observatoire de Genève, Université de Genève, Chemin Pegasi 51, 1290 Versoix, Switzerland

Because of gravitational lensing, galaxy clusters bend and magnify light from sources behind them. We can use this phenomenon as a ‘cosmic telescope,’ observing galaxies hidden behind dense clusters at much higher resolutions than we would otherwise. The goal of this project was to use this to study the integrated properties of high-redshift galaxies observed by the James Webb Space Telescope (JWST) and the Hubble Space Telescope (HST). We extracted photometry at various scales from newly released JWST and HST images in order to calculate stellar mass and star formation rate for those galaxies and hence create a catalog of masses for the 18 strongly lensed high red-shift target galaxies while also comparing the redshift evolution of the the star formation main sequence with previously existing results. We took advantage of lensing to be able to observe galaxies which were otherwise too faint. We also looked into the behaviour of clump masses for clumpy galaxies and tried to deduce visible trends from the analysis.

1 INTRODUCTION

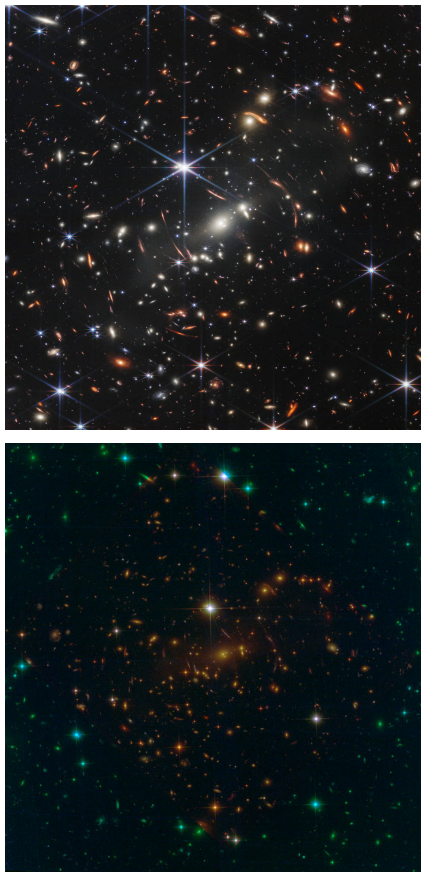


FIGURE 1. This image depicts the 4.6 billion-year-old galaxy cluster SMACS 0723, with many more galaxies in front of and behind it. The top image was captured using JWST’s NIRCam, using near and mid-infrared filters while the bottom image was previously captured using HST in the optical going slightly into infrared.

SMACS 0723 (SMACS J0723.3-7327) is one of the first targets imaged by NASA’s James Webb Space Telescope (JWST). At a distance of 4.24 billion light-years, the massive cluster is located in the southern constellation Volans (the Flying Fish).

One of the goals of the James Webb Space Telescope’s launch was to peer into galaxies as they appeared in the early universe. Massive galaxies clusters, such as SMACS 0723, allow astronomers to see some of these galaxies, whose light is magnified and bent by the sheer mass of the foreground clusters.

Hubble had previously imaged SMACS 0723. While the images appear to be similar, the JWST image is more detailed, providing an unprecedented view of thousands of distant galaxies. Because of its superior light gathering power, the new space telescope was able to capture many more distant galaxies in the same field, including the faintest infrared objects ever seen. (See FIGURE 1).

It has been considered as the target cluster for the project. The resolution of a telescope is determined by the size of its mirror and the wavelength of light being observed. Except when it comes to wavelength: the longer the wavelength of light, the lower the resolution of the telescope. JWST detects infrared light, which has a longer wavelength than Hubble does. When we compare the range of observation in the spectrum of the HST and JWST, we can see that for longer wavelengths, such as near IR, the JWST will produce much higher resolution images than the HST, but when we observe the same object at a wavelength in the ultraviolet or visible, the HST will produce images as good as the JWST.

The Point Spread Function (PSF) is an optical instrument’s response to an impulse. It describes how much the instrument has distorted the observed light distribution. Knowing the PSF is therefore essential in astronomy for morphometric and photometric measurements. The PSF has a six fold symmetry for JWST while for HST it is four fold. Critical elements of an efficient optics system is a high quality well modeled, stable PSF.

When we compare PSF values for HST and JWST, we see that for comparable wavelengths (JWST F090W vs. HST F105W), the PSF full width half maximum value for JWST

is nearly three times lower than for HST, implying that the images are sharper with JWST.

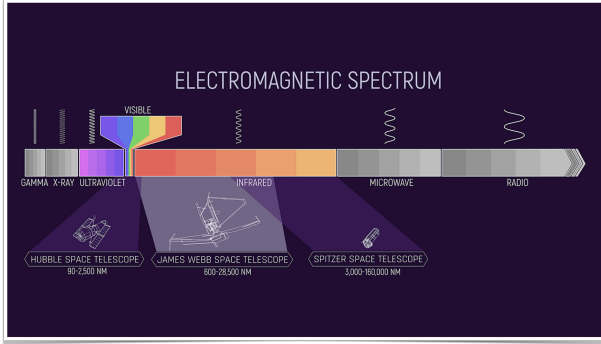


FIGURE 2. Image(webbtelescope.org) This image depicts the electromagnetic energy spectrum, focusing on the portions detected by NASA's Hubble, Spitzer, and Webb space telescopes. The infographic shows how much of the electromagnetic spectrum each of these telescopes covers, as well as the total coverage. Other telescopes detect different parts of the electromagnetic spectrum, and these scientific instruments work together to provide a more complete picture of the universe and how it works.

1.1 Exploring some theoretical concepts

Gravitational Lensing : We are working on a "lensing cluster" in our project. Gravitational lensing is an important concept to understand in order to understand the behaviour of such a cluster. Normal lenses, such as those found in magnifying glasses or spectacles, work by bending light rays as they pass through them in order to focus the light somewhere. This process is known as refraction (such as in your eye). Gravitational lensing is a similar effect of Einstein's general theory of relativity - simply put, mass bends light. The gravitational field of a massive object will extend far into space, bending and refocusing light rays that pass close to it (and thus through its gravitational field (see FIGURE 3). The more massive an object, the stronger its gravitational field, and thus the greater the bending of light rays - just as using denser materials to make optical lenses results in more refraction. As the light passes close to the foreground cluster, the images of distant, lensed galaxies are stretched and pulled into arcs.

The observer may then see multiple distorted images of the same source, the number and shape of which are determined by the relative positions of the source, lens, and observer, as well as the gravitational well of the lensing object.

A point-like gravitational lens, unlike an optical lens, produces a maximum deflection of light passing closest to its center and a minimum deflection of light passing farthest from its center. As a result, a gravitational lens has a focal line rather than a single focal point. When the lensing mass is complex (such as a galaxy group or cluster) and does not cause a spherical distortion of spacetime, the source will look like partial arcs scattered around the lens.

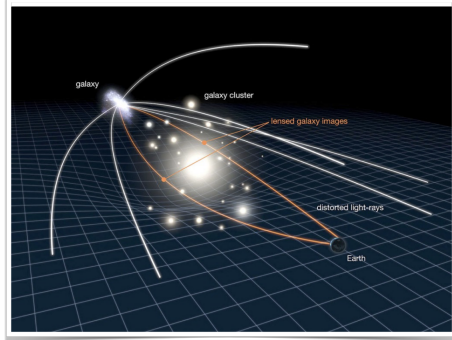


FIGURE 3. Image(NASA/ESA) Illustration explains effect of gravitational lensing on imaging objects beyond a strong gravitational field

The glass lens collects light across its surface, which is usually much larger than the pupil of a human eye. As a result, a lens can increase illumination. Furthermore, when a light ray passes through a glass lens, its path is bent. Essentially, the path bends when light passes from air to glass and then back again. This bending is referred to as refraction, and the typical lens shape focuses the light to a single point. When we look at the collected light, our view of the object can be magnified or reduced depending on the distances involved, both between the object and the lens and between the lens and our eyes. Finally, a glass lens can amplify and magnify light from an object.

Another interesting effect is that the images become inverted beyond the critical line for the galaxy. A critical line simply the region at which the image's amplification reaches infinity.

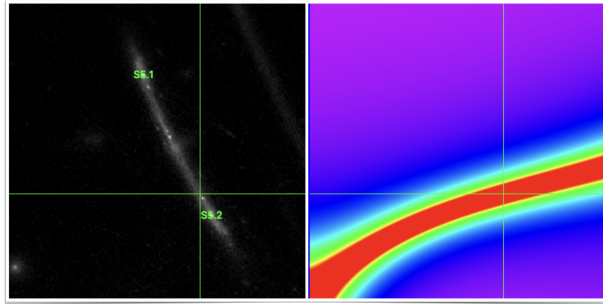


FIGURE 4. Left: JWST image of the same galaxy in band F090W; Right: This is an amplification map of the galaxy marked S5.1/2. The amplification of the image does not decrease to zero even when you are far away from the galaxy.

Star Formation Main Sequence(SFMS) : Star formation rate quantifies the number of stars formed in a galaxy over a given period of time and this star formation rate is said to correlate with the stellar mass for star-forming galaxies and this relation is referred to as the galaxy main sequence or the star formation main sequence. The relation exists at both low ($z < 1$) and high ($z \geq 1$) redshift and is recovered in optical, infrared and radio observations .

As shown later in the report, we have tried to verify the SFMS by extracting the photometry and trying to fit the Spectral En-

ergy Distribution on it for the target galaxies.

Galaxy clumps and their importance : Deep Hubble Space Telescope (HST) observations and ground-breaking morphological analysis of distant star-forming galaxies have revealed that galaxies at the peak of cosmic star formation activity are irregular and clumpy, rather than conforming to the Hubble classification.

HST data has revealed a population of clumpy galaxies that do not appear as chains, but rather as more circular groups of clumps over time. "Clump clusters" are the name given to these.

There are a few key differences between clump clusters and modern irregular galaxies. Clump clusters are typically much larger, and today's irregulars would appear irregular no matter which way they were viewed. The similarity between clump clusters and chain galaxies suggests that they are the same object seen from different perspectives. This implies that the clumps are irregularly distributed in relatively thin disks that appear as chains from the edge.

Further study of clumpy galaxies confirms that they are very young galaxies with a lot of star formation occurring in the massive clumps, which may be embedded within a slightly older, smoother distribution of stars. They are most likely an early stage in the development of most galaxies due to their prevalence. By analyzing these clumps, we hope to learn a lot more about these galaxies. From asymmetric clumpy galaxies to symmetric clumpy galaxies, clumpy galaxies dominated by a bright central clump, and finally spiral galaxies, there appears to be a rough developmental sequence. Other clumpy galaxies may join together to form elliptical galaxies. By comparing the numbers and properties of these different types of galaxies, we will be able to confirm or refute this view and gain a better understanding of the origins of the galaxy population. Giant, star-forming clumps are a common feature of high-redshift star-forming galaxies, and they play a significant role in shaping their chaotic morphologies.

2 Methods

Identifying contours : The first step would be to identify all of the galaxies based on their celestial coordinates taken from Claeysens et al., 2022. We primarily used DS9 for this task. The contours of the target galaxies are then marked using a 3σ threshold, where σ represents the root mean square (RMS) values or noise of the area around each galaxy.

As we can see in FIGURE 5, choosing 3σ was a trial-and-error process because 2σ caused the images to include unwanted bright objects and 4σ did not completely include all galaxies. The contour marking was done on image corresponding to the JWST F090W (9022.9 Å).

It is important to note that these contours were then used as references for all other bands considered for the project.

Contamination removal model : Despite having used the 3σ contour method, the true flux of the galaxies get affected

due to the presence of bright objects in close vicinity to them. Thus it is imperative that we use a model to remove these bright unwanted objects from the images. The model used for accomplishing this task uses the properties of sersic profiling of galaxies.

The removal of these bright objects enable us to move closer to measuring the true flux of the target galaxies.

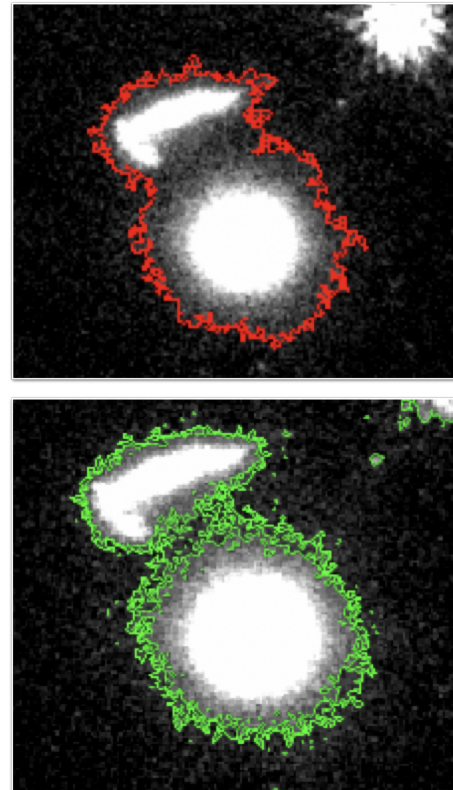


FIGURE 5. Comparison between 2σ (up) and 3σ (down) contours. Clearly, background elimination turns out to be much better for the 3σ contour

An initial model is created with predefined values for eccentricity, amplitude, sersic index, and other features for a dummy galaxy. Because the majority of these unwanted bright objects have a circular or elliptical shape, the parameter values are taken as one would for such galaxies. The model then finds the best estimate of the same parameters based on the RMS values and polygon coordinates defining the unwanted galaxy's periphery. To finally extract an image free of contamination, we subtract the modelled galaxy from the original image, and the residual is our desired product (see FIGURE 6[4]).

To reduce the number of images to process, all unwanted contamination for all galaxies in a given band was removed. This raises the possibility of subtracting noise multiple times because the model removes noise from the entire image rather than just around the object under consideration. However, the RMS values were negligible when compared to the mean values in the background, so multiple noise subtraction had

no discernible effect on the flux in the images.

Lensing Correction : Given the amplification effect of gravitational lensing, the observed flux of the target regions must be divided by the amplification. It is important to note that we used differential amplification because our sources were subject to differential amplification. This means that

This project chose 18 lensed galaxies at redshifts 1 to 8 from the lensing cluster field SMACS0723 with an effective number to be 36 as many galaxies have multiple images due to lensing. The reason for this choice was that these galaxies are all reported in Claeysens et al. (2022), so we used them all in order to have a statistical sample. A reliable redshift measurement and/or a high lensing magnification is also helpful in the analysis.

We then created a catalog with columns being Original data , Lens corrected original data, Residual data , residual lens corrected data in order for all wavelengths taken under consideration and rows being values for each of the regions identified. The celestial coordinates for all the regions were referred from [Claeysens]

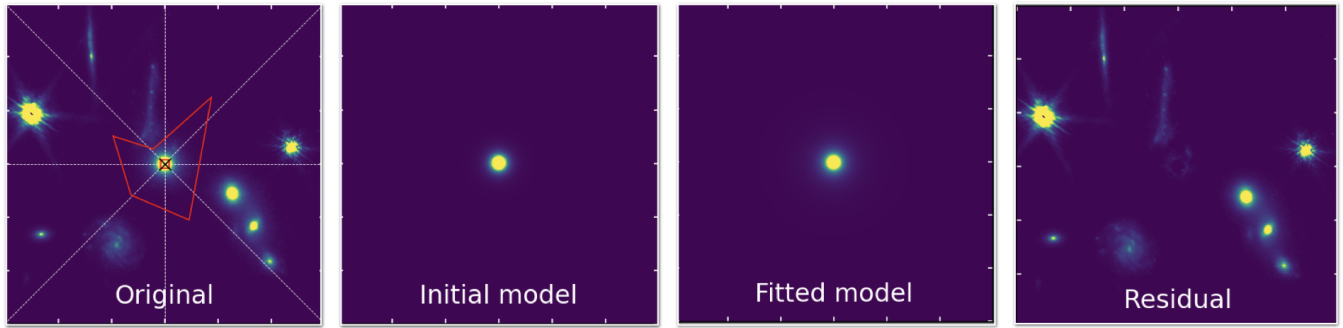


FIGURE 6. [1]: The original object (in yellow) with a polygon defining the region (in red);[2]: The initial model with dummy parameter values;[3]: The fitted model with best estimate of the parameters;[4]: the residual formed after subtraction of the fitted model from the original region selected

The wavelength bands considered for the project can be summed up in the following table [Claeysens] :

Filter	Rest Wavelength (Å)	PSF FWHM
HST F435W	4329.8677	0.120
HST F606W	5921.8911	0.120
HST F814W	8045.5327	0.120
JWST F090W	9022.92216966	0.050
HST F105W	10551.047	0.160
HST F125W	12486.06	0.180
HST F140W	13922.907	0.190
JWST F150W	15007.454908178	0.060
HST F160W	15369.176	0.190
JWST F200W	19886.47813979	0.068
JWST F277W	27577.95876438	0.110
JWST F356W	35682.2776384	0.130
JWST F444W	44036.71097715	0.140

3 Analysis

SED Fitting and Analysis: Galaxies emit electromagnetic radiation at all frequencies and wavelengths. The main way astronomers study distant galaxies and learn about their formation and evolution is through the analysis of their radiation. The Spectral Energy Distribution(SED) is the distribution of energy(flux) over wavelength/frequency. The reason

we considered the amplification of each pixel on the image rather than the average amplification of the image. To begin lensing correction, we used Python code to import all residual (contamination-free) images for all bands under consideration, as well as the corresponding amplification map for all regions.

This project chose 18 lensed galaxies at redshifts 1 to 8 from the lensing cluster field SMACS0723 with an effective number to be 36 as many galaxies have multiple images due to lensing. The reason for this choice was that these galaxies are all reported in Claeysens et al. (2022), so we used them all in order to have a statistical sample. A reliable redshift measurement and/or a high lensing magnification is also helpful in the analysis.

We then created a catalog with columns being Original data , Lens corrected original data, Residual data , residual lens corrected data in order for all wavelengths taken under consideration and rows being values for each of the regions identified. The celestial coordinates for all the regions were referred from [Claeysens]

we perform SED fits is to get the stellar mass and the star formation rate of the galaxies. An SED is similar to a black-body curve and is made up of spectra or photometric data observations of a star/galaxy. For our analysis,a final photometric catalogue was created with red-shifts along with lens corrected fluxes and errors to be used as input for the SED analysis of the target galaxies, which estimates their ages,

masses, and extinction. We have access to spectroscopic redshift for most of our sources, which constrain the SED fit. For the other few sources which only have photometric redshift, we fit the redshift ourselves. Since the technique rests on assumptions such as the galaxy star formation history (SFH) and dust attenuation law there is an impact on the accuracy of derived physical properties from SED modeling. For modeling galaxy spectra and fitting spectroscopic and photometric observations, we used BAGPIPES (Bayesian Analysis of Galaxies for Physical Inference and Parameter Estimation) for which assumed the same priors and star formation history for all the regions while in reality these assumptions change according to the nature of the galaxies. Since we have a lot of sources to fit as we want a statistical sample, we cannot study them one by one to constrain the priors better. An important prior to note is the Delayed star formation model or the Delayed tau model :

$$SFR \sim t * e^{-t/\tau}$$

where, SFR is the star formation rate, t is the time and tau is the fitting parameter.

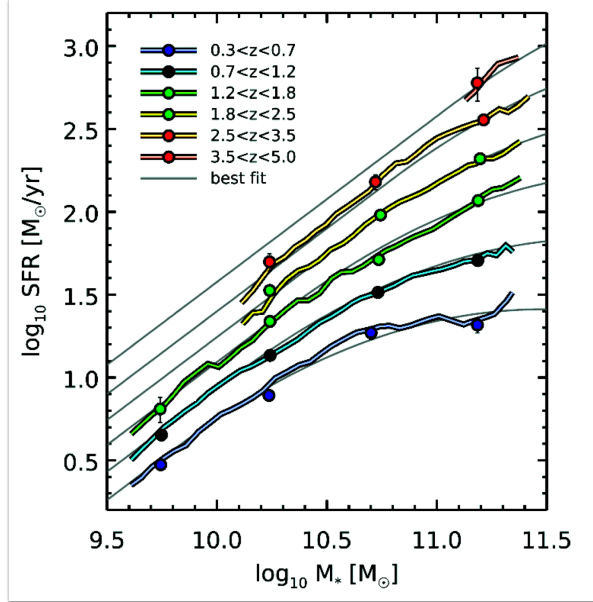


FIGURE 7. Expected redshift evolution of the star formation main sequence on log scale , C. Schreiber et al, 2015

The dust model from Calzetti et al (2000) was considered as the dust attenuation law for the fitting. Having a look at a few SED plots (see FIGURE 9) for different galaxies we see that SED fits are better for smaller blobs of galaxies and the

nature of the plots are highly dependent on age and red-shift of the galaxies.

SFR Vs Stellar Mass: Having obtained the stellar mass and star formation rate of galaxies from the SEDs, we can now verify the Star Formation Main Sequence and also observe the redshift evolution of the same for the galaxies that we took into consideration. In FIGURE 7 we see the expected SFMS plot while FIGURE 8 shows the plot we produced using our data and hence we note that the galaxies indeed satisfy the expected redshift evolution

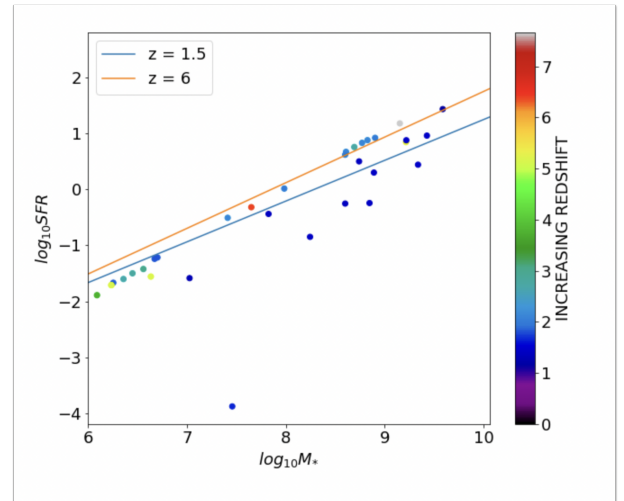


FIGURE 8. Verified redshift evolution of the star formation main sequence, on log scale.

For higher redshift values the star formation rate is higher for the same stellar mass of galaxies as expected. The blue line is the normalisation line at redshift 1.5 while the orange line is the normalisation line at redshift 6.

Plotting of Clump Masses: We first looked at the relative percentage of individual clump masses with respect to the total mass of the galaxies.(see FIGURE 10)

We then observe the behaviour of these clumpy galaxies by plotting the relative flux of these clumps with respect to the total true flux received from the galaxies comprising said clumps.(see FIGURE 11)

The main trend observed is that clumpiness increases in the UV and decreases as wavelength increases. At redder wavelengths, the galaxy appears less clumpy. The clumpiness in rest-frame UV wavelengths and thus massive stars from recent star formation suggests that a significant fraction (~ 0.5) of recent star formation occurs in the observed clumps.

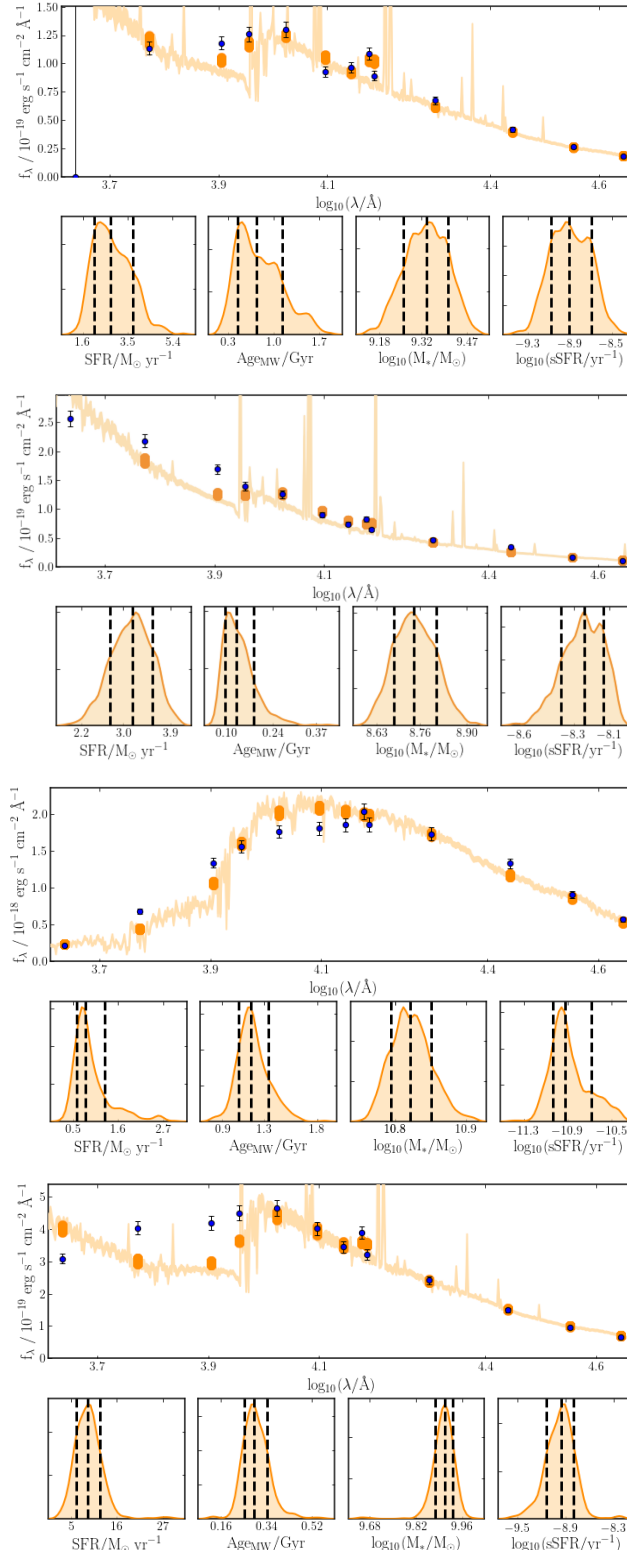


FIGURE 9. A few examples of SED fits for target galaxies in the lensing cluster SMACS0723 used to infer the Star formation rate to Stellar Mass Ratios and Age in Gigayears . The SED's nature is determined by the redshift and age of galaxies out of many other factors. As previously stated, SEDs appear to fit better for smaller blobs of galaxies. This could be due to contamination effects and a lack of flux from larger galaxies. The missing flux can be explained by the use of a uniform template for sigma contours (reference image in F090W filter) during the identification of 36 regions on DS9. As a result, the reference contours may fail to cover the entire extent of the aforementioned regions, resulting in missing flux. Some SEDs have a distinct dip just before 4000 Å, which is known as the Balmer Break. In the last SED fit we see that the star formation rate is highly overestimated as compared to the expected values. This is because the SED in question has been plotted for the flux catalog of the galaxy before lens correction and removal of contamination implying the importance of the same. The errorbars in some plots running from 0 to ∞ indicate that no flux was detected at those wavelengths/filters.

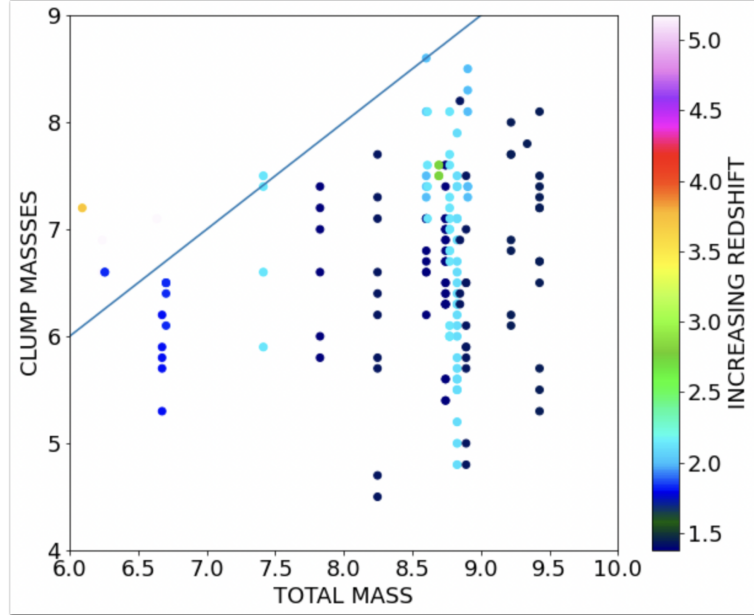


FIGURE 10. Stellar masses(in log) of high-redshift clumps plotted as a function of the stellar mass of their host galaxy. In comparison to the star clusters identified in local galaxies, the inferred clump masses in high-redshift galaxies are, on average, significantly higher than those in local galaxies also shown with the exception of some star clusters in the most intensively star-forming nearby galaxies.

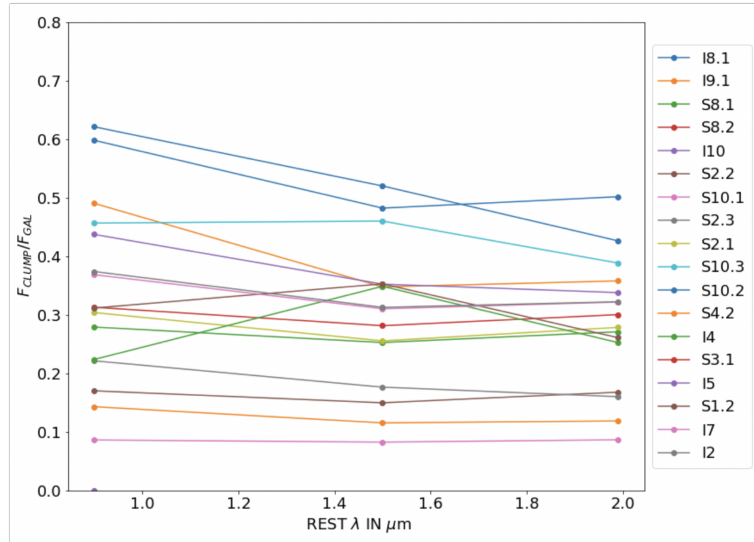


FIGURE 11. Plot $F_{\text{clump}}/F_{\text{galaxy}}$ VS Rest Wavelength. With some discrepancies the general trend observed is that the clumps dominated more in the bluer wavelength than the red ones.

4 Conclusion

Having done multiband photometry across 13 wavelengths for 36 regions around the lensing cluster SMAC0723 we can derive a few inferences. From the recreation of the redshift evolution of star formation main sequence The star formation rate indeed increases for the same stellar mass at higher redshift. The clumpiness of galaxies is higher in the the blue wavelengths as they trace the star forming regions while the redder wavelengths trace the older stellar population within a galaxy. Inferred clump masses in high-redshift

galaxies are, on average, significantly higher than those in local low redshift galaxies. We realise the importance of removal of contamination around galaxies and Lensing correction while analysing images as otherwise we overestimate physical properties of galaxies drastically and produce erroneous results. Despite having used some correction methods there were some shortcomings that we noticed during the analysis. Having considered constant priors (mainly the star formation history and dust attenuation laws), the SED fitting is not as accurate due to its strong dependence on the nature

of the galaxies. We could not study them one by one to better constrain the priors because we had a large number of sources to fit as a statistical sample. Owing to the same reason, we used one reference contour set for all the chosen regions in the F090W filter which in turn led to some reduction in accuracy of flux measurements especially in the redder wavelengths. However, the flux for bluer wavelengths seem to not be affected by given constraints.

5 References

Zavadsky,2017, Miroslava Dessauges et al, On the Stellar Masses of Giant Clumps in Distant Star-forming Galaxies,The Astrophysical journal,<https://doi.org/10.48550/arXiv.1702.00055>

Claeyssens, Adélaïde et al, Star formation at the smallest scales; A JWST study of the clump populations in SMACS0723,MNRAS <https://doi.org/10.48550/arXiv.2208.10450>

Messa2022, Matteo Messa et al, Multiply lensed star forming clumps in the A521-sys1 galaxy at redshift 1, Monthly Notices of the Royal Astronomical Society,<https://doi.org/10.48550/arXiv.2208.02863>

Nagy2021, David Nagy et al., Radial profiles of lensed $z \sim 1$ galaxies on sub-kiloparsec scales, Astronomy Astrophysics Journal, <https://doi.org/10.48550/arXiv.2109.06206>